Bartram et al. BMC Medical Genetics (2017) 18:53
DOI 10.1186/s12881-017-0416-5

BMC Medical Genetics

RESEARCH ARTICLE Open Access

Characterization of a splice-site mutation in the tumor suppressor gene *FLCN* associated with renal cancer

Malte P. Bartram[1†], Tripti Mishra[1†], Nadine Reintjes[2], Francesca Fabretti[1], Hakam Gharbi[1], Alexander C. Adam[3], Heike Göbel[3], Mareike Franke[4,5], Bernhard Schermer[1,6,7], Stefan Haneder[4], Thomas Benzing[1,6,7], Bodo B. Beck[2] and Roman-Ulrich Müller[1,6,7*]

Abstract

Background: Renal cell carcinoma is among the most prevalent malignancies. It is generally sporadic. However, genetic studies of rare familial forms have led to the identification of mutations in causative genes such as *VHL* and *FLCN*. Mutations in the *FLCN* gene are the cause of Birt-Hogg-Dubé syndrome, a rare tumor syndrome which is characterized by the combination of renal cell carcinoma, pneumothorax and skin tumors.

Methods: Using Sanger sequencing we identify a heterozygous splice-site mutation in *FLCN* in lymphocyte DNA of a patient suffering from renal cell carcinoma. Furthermore, both tumor DNA and DNA from a metastasis are analyzed regarding this mutation. The pathogenic effect of the sequence alteration is confirmed by minigene assays and the biochemical consequences on the protein are examined using TALEN-mediated transgenesis in cultured cells.

Results: Here we describe an *FLCN* mutation in a 55-year-old patient who presented himself with progressive weight loss, bilateral kidney cysts and renal tumors. He and members of his family had a history of recurrent pneumothorax during the last few decades. Histology after tumor nephrectomy showed a mixed kidney cancer consisting of elements of a chromophobe renal cell carcinoma and dedifferentiated small cell carcinoma component. Subsequent *FLCN* sequencing identified an intronic c.1177-5_-3delCTC alteration that most likely affected the correct splicing of exon 11 of the *FLCN* gene. We demonstrate skipping of exon 11 to be the consequence of this mutation leading to a shift in the reading frame and the insertion of a premature stop codon. Interestingly, the truncated protein was still expressed both in cell culture and in tumor tissue, though it was strongly destabilized and its subcellular localization differed from wild-type FLCN. Both, altered protein stability and subcellular localization could be partly reversed by blocking proteasomal and lysosomal degradation.

Conclusions: Identification of disease-causing mutations in BHD syndrome requires the analysis of intronic sequences. However, biochemical validation of the consecutive alterations of the resulting protein is especially important in these cases. Functional characterization of the disease-causing mutations in BHD syndrome may guide further research for the development of novel diagnostic and therapeutic strategies.

Keywords: FLCN, Folliculin, BHD syndrome, Birt-Hogg-Dubé syndrome, Kidney cancer, Renal cell carcinoma, Proteasome, Lysosome

* Correspondence: roman-ulrich.mueller@uk-koeln.de
†Equal contributors
[1]Department II of Internal Medicine and Center for Molecular Medicine Cologne, University of Cologne, Kerpener Str. 62, 50937 Cologne, Germany
[6]Cologne Excellence Cluster on Cellular Stress Responses in Aging-Associated Diseases (CECAD), University of Cologne, Cologne, Germany
Full list of author information is available at the end of the article

Background

Birt-Hogg-Dubé syndrome (BHD) is a rare autosomal dominant inherited tumor syndrome caused by mutations in the *FLCN* gene [1, 2]. The disease is characterized by a triad of renal cell carcinoma, benign skin tumors (fibrofolliculomas) and pulmonary cysts that predispose to recurrent pneumothorax. Since the clinical presentation is highly variable even within families, it is likely that BHD syndrome is an underdiagnosed disorder. About 600 families with *FLCN* mutations have been reported. Increasing awareness of the disease results in a steadily growing number of diagnoses [3–5]. The prevalence of the clinically most important consequence of BHD syndrome, renal cell carcinoma, varies between studies from 12 to 34% [6, 7]. In line with Knudson's hypothesis loss of heterozygosity or somatic mutations have been observed in renal tumor tissue [8, 9]. Due to the strongly increased risk of renal cell carcinoma in patients with BHD syndrome and the occurrence of renal tumors in rodent models of the disease FLCN can be considered a tumor suppressor protein. On the molecular level, FLCN has been linked to a multitude of pathways including mTOR, AMPK signaling, the VHL/HIF/VEGF axis, TGFb signaling, autophagy and cilia (reviewed in [10]; [11–20]) although the exact function is incompletely understood and is subject to intense research. Currently 159 disease causing FLCN mutations have been reported in the Human Gene Mutation Database (HGMD professional; assessed 2016.4; https://portal.biobase-international.com/hgmd/pro/).

Matchable numbers can be obtained from a publicly available database - the Folliculin Sequence Variation Database [4] - hosted online by the Leiden Open Variation Database (LOVD), which currently contains 152 FLCN mutations; data freeze January 2017; https://www.bhdsyndrome.org/). Small deletions or duplications, small insertions and small insertions/deletions (indels) that predominantly result in a frameshift ($n = 80$; ca. 50%, all numbers here refer to HGMD), nonsense mutations ($n = 23$; ca. 15%), gross (genomic) deletions or amplifications ($n = 22$; ca. 14%) and (intronic) splice mutations ($n = 21$; ca. 13%) account for the vast majority of cases (ca. 92%), while missense mutations are comparatively rare ($n = 13$; ca. 8%). The reported frequency of gross (genomic) deletions/amplifications in BHD makes MLPA analyses (multiplex ligation-dependent probe amplification) a useful tool in the diagnostic work of suspected BHD cases. Whilst the consequences of sequence alterations in the coding regions are often obvious, the pathogenic potential of many splice mutations and (intronic) variants likely affecting splicing found in BHD syndrome - including c.1177-5_-3delCTC - has not been studied well beyond in silico analyses [4, 5, 21].

Methods

Sanger sequencing

After obtaining written informed consent from the index patient, mutational analysis of the *FLCN* gene was performed by exon PCR of all 11 coding exons. Primer sequences for the exons and adjacent intron-exon borders were designed with the Exon Primer software (https://ihg.helmholtz-muenchen.de/ihg/ExonPrimer.html). For analyses of formalin-fixed paraffin-embedded tissue sections primers generating appropriate short amplicons (150 bp) were selected. Primer sequences and PCR conditions are available on request. Purified PCR products were sequenced by BigDye terminator ready reaction kit v.1.1 (Life Technologies), using a 3500 Genetic Analyzer (Applied Biosystems). Resulting sequences were evaluated with the Sequence Pilot ™ software (JSI Medical Systems GmbH, Germany).

Cell lines

HEK293T (gift from Brian Seed (Boston)), UOK257 (gift from Laura Schmidt and Michael Pollak (NIH)) and IMCD (from ATCC) cells were maintained in DMEM + 10% fetal bovine serum (FBS) at 37 °C. RPE-1 cells (from ATCC) were maintained in DMEM/F12 + 10% fetal bovine serum (FBS) at 37 °C.

Construction of FLCN expression plasmids, minigenes and minigene assay

To generate expression plasmids of FLCN WT PCRs using sequence specific primers that generate a 5′ Mlu1 site and 3′Not1 site to clone the PCR products into a modified pcDNA6 vector (Invitrogen) were used using standard techniques (fp: 5′-cgcgggacgcgtATGAA TGCCATCGTGGCTCTC-3′; rp 5′-gcggggcggccgccTC AGTTCCGAGACTCCGAGGC-3′). The plasmid expressing the FLCN patient mutation (missing exon 11) was generated using overlap extension PCRs. All constructs were verified by sequencing.

The minigene-11 construct containing parts of human FLCN exon 10, intron 10 and parts of exon 11 was cloned via PCR using a forward primer that is located in exon 10 and a reverse primer located in exon 11 into a modified pcDNA6 vector (Invitrogen). The minigene-2 construct, containing parts of exon 10, intron 10, exon11, intron 11 and parts of exon 12 a forward primer located in exon 10 and a reverse primer located in exon 12 was used. Both, the WT and the patient mutation constructs were cloned by PCR using patient genomic DNA derived from lymphocytes as a template. WT and mutant clones were identified by Sanger Sequencing. All plasmids were verified by sequencing. Afterwards the plasmids were transfected into mouse cells (IMCD) to prevent that endogenous human FLCN interferes with the analysis of the minigenes. 24 h after

transfection RNA was extracted from the cells using standard methods and cDNA was generated (ABI High-Capacity cDNA Kit). Afterwards PCRs were performed and the PCR products resolved on an agarose gel (primers for minigene-1: fp 5′- tgggtgccccttctttc rp 5′- gctgagccccaggaagtt; primers for minigene-2: fp 5′- aac caggtgatctggaaa rp 5′- cactggtcaccacaaactcg. The indicated bands/PCR products were further analysed by Sanger sequencing.

AAV-CAGGS-EGFP-hFLCN transfection in HEK293T cells to generate TALEN cells

The sequences of FLCN WT and the patient mutation missing exon11 were subcloned into a modified AAV-CAGGS-EGFP vector (a TALEN-based vector, Addgene 22212) in a way that a GFP fusion protein is created. The constructs were confirmed by sequencing. HEK293T cells were transfected with 1 μg AAV-CAGGS-EGFP-hFLCN WT or 1 μg AAV-CAGGS-EGFP-hFLCN Mut) along with 0.5 μg hAAVS1 1 L TALEN and 0.5 μg hAAVS1 1 TALEN nuclease plasmids using the calcium phosphate transfection method. 48 h after transfection, cells were kept in 2 μg puromycin selection. Few colonies were found after selection for 2 weeks. The colonies were then expanded and further analysed by Western Blot and imaging experiments.

MG-132 treatment and chloroquine treatment

Cells were treated with 10 μM MG-132 (Calbiochem, cat. # 474790) for 2 h and 50 μM Chloroquine (Sigma, cat. # C6628) for 24 h respectively. After treatment, cells were harvested in 10 ml ice-cold PBS and then centrifuged at 200 *g* for 5 min at 4 °C. The supernatant was discarded and the pellet was resuspended in 300 μl IP buffer (1% Triton-X-100, 20 mM Tris HCl pH 7.5, 50 mM NaCl, 25 mM NaF, 12.5 mM $Na_4P_2O_7$, 2 mM Na_3VO_4, PMSF (44 μl/10 ml)) and incubated for 15 min on ice. Lysates were then centrifuged at 20800 *g* for 30 min at 4 °C. 200 μl supernatant was transferred to a new 1.5 ml tube for further use. 40 μl of this supernatant was taken and boiled with 40 μl 2× Laemmli buffer at 95 °C for 5 min followed by Western blot analyses (mouse anti-GFP (St. Cruz, sc-9996) and mouse anti-Tubulin (clone E7, DSHB).

Fluorescence imaging

Stably integrated AAV-CAGGS-EGFP-hFLCN WT and AAV-CAGGS-EGFP-hFLCN Mut cells were fixed in 4% PFA for 15 min at room temperature. PFA was discarded and cells were washed 3 times with PBS (supplemented with Ca^{2+} and Mg^{2+}). Mounting was performed using Prolong Gold with DAPI (Invitrogen). Images were visualized using Axiovert 200 microscope (objective: C-Apochromat × 63/1.22 W).

siRNA experiments

RPE-1 cells were transfected using Lipofectamine 2000 (Invitrogen) according to the manufacturer's protocol with a final siRNA concentration of 25 nmol/μl. 21mer siRNA oligos were purchased from Biomers (Ulm, Germany). The following sequences were used: Control siRNA: AAATGTACtgcgcgtggagac; FLCN siRNA#1 aug gugaugaugcuguaccttt. The second FLCN siRNA was purchased from ThermoFisher Scientific (USA) as ready annealed siRNA duplex (J-009998-05-0005).

Generation of cell lysates and Western Blot

Whole cell lysates of the RPE-1 cells transfected with the control or FLCN targeting siRNAs were lysed directly in SDS-PAGE sample buffer (1× Laemmli). Equal amounts of protein were resolved using were resolved by SDS-PAGE, blotted on to PVDF-membranes and visualized with enhanced chemiluminescence after incubation of the blots with the respective antibodies (rabbit anti-FLCN antibody (CellSignaling, #3697) and mouse anti-actin (Millipore, MAB1501R).

Generation of UOK257 cells reexpressing FLCN WT

To reexpress FLCN in the FLCN deficient UOK257 cell line F9. FLCN WT was cloned using standard techniques into a modified pENTR1A vector (Invitrogen) and afterwards recombined into pLenti6.3 using the Gateway technology (Invitrogen). pLenti6.3-emGFP served as control. After virus production in HEK293T cells the UOK257 cells were transduced for 24 h and afterwards selected using blasticidin. To validate the FLCN antibody the FLCN and GFP expressing cell lines were seeded onto coverslips and IHC stained using the rabbit anti-FLCN antibody (CellSignaling, #3697).

Immunohistochemical staining

Four μm sections were cut from paraffin embedded, formalin-fixed tissue blocks, mounted on silane coated slides, dried and deparaffinised by routine techniques in xylene and rehydrated in ethanol (100, 100, 90, 70, 50%). Sections were then washed in Tris–HCl buffer (pH 8.0) before incubation with primary antibody (anti-Folliculin, CellSignaling #3697, 1:20, pretreatment: citrate puffer (pH 6.0),). The incubation was performed over night at 4 °C. Labeling was detected semiautomatically by DAKO TechMate™ 500 Plus with the DAKO REAL™ Detection System using the streptavidine-biotin system according to manufacturer's protocol (Dako REAL™ Biotinylated Secondary Antibodies: goat anti-mouse and anti-rabbit immunoglobulins, Dako REAL™ streptavidine peroxidase, Dako REAL™ AEC/H2O2 Substrate Solution, Dako REAL™ Blocking Solution, Dako REAL™ Buffer Kit). Sections were washed (3 times 5 min in PBS), counterstained with

haematoxylin and finally mounted in Aquatex (Merck, Darmstadt, Germany).

Results

The 55-year-old index patient presented to our emergency department in a reduced condition with night sweats, anemia, weight loss and progressive edema of both legs. In the medical history bilateral lesions of both kidneys had been known for about 20 years. These had been classified as angiomyolipomas due to their radiological aspects and led to the clinical diagnosis of oligosymptomatic tuberous sclerosis. Due to several episodes of spontaneous macroscopic hematuria suspicion of an increased risk of bleeding had prevented biopsies of the lesions so far. In addition, the patient reported several episodes of pneumothorax in the past as well as the occurrence of pneumothorax in other family members.

Cross-sectional imaging revealed dramatically enlarged kidneys (22 cm in length) with multiple tumorous lesions consistent with angiomyolipomas as well as an unclear 1.2x1.0 cm lesion on the lower pole of the left kidney (Fig. 1a). In addition several suspicious retroperitoneal lymph nodes were seen. Owing to their enormous size the kidneys compressed the pelvic vessels explaining the edema of the legs, echocardiography revealed a normal ejection fraction and no valvular disease. Furthermore, hepatosplenomegaly – most likely due to concurrent osteomyelofibrosis - and several lung cysts and pulmonary nodules were seen in a CT of the chest (Fig. 1b and c).

Nephrectomy of the left kidney was performed (Fig. 1d) to allow for histological examination of the lesions and relieve the compression of the inguinal vessels. Open surgery revealed peritoneal metastases. Pneumothorax of the left lung occurred as a perioperative complication and was treated with a chest tube. Histopathological work up of the renal tissue showed that the whole kidney was tumorous (Fig. 1d) with features of a chromophobe renal cell carcinoma (Fig. 1e (right side of the panel) and Additional file 1: Figure S1a-c). Beside the chromophobe carcinoma there was a second tumor entity consisting of small carcinoma cells with nuclear pleomorphism and atypical mitoses already invading the blood vessels (Fig. 1e (left side of the panel), Fig. 1f and Additional file 1: Figure S1c). Since the chromophobe carcinoma showed signs of dedifferentiation towards the small cell carcinoma component, we speculate that these cells might originate from the chRCC by acquiring further genetic alterations. Staining of several markers like CKAE1/3, CK7, TTF-1 and CD-*X*2 of the small cell carcinoma lesions were negative, indicating that these cells have no extrarenal origin (data not shown). There were no signs for lesions consistent with oncocytoma.

Histopathological work up of one peritoneal metastasis showed features of the small cellular tumor component (Additional file 1: Figure S1c and d), suggesting that these cells might contribute to the severe and aggressive tumor phenotype in our patient. Consistent with this observation, these cells showed a very high proliferation index analyzed by Ki-67 staining (Additional file 1: Figure S1f and g). Further immunohistological analysis of the metastastic tissue showed no staining for TTF-1, CD10 or ChrA (data not shown) as expected since the scattered small cell component that is seen throughout the tumor appears to be a less differentiated part of the chRCC. Soon after surgery hemodialysis was initiated due to end-stage renal failure. However, the patient died shortly afterwards as a consequence of the advanced stage of the metastatic tumor disease.

The co-occurrence of chromophobe renal cell carcinoma with familial recurrent pneumothorax made us suspect Birt-Hogg-Dubé syndrome in this family. Sanger sequencing of lymphocyte DNA was performed and revealed a previously reported heterozygous intronic three nucleotide deletion c.1177-5_-3delCTC just upstream of exon 11 (Fig. 2).

In silico analyses by several bioinformatic tools predicted this variant to be likely pathogenic. Splicing assessment using the alamut visual 2.7 indicated a significant weakening of the native acceptor site of exon 11, however neither generation of a novel acceptor site nor exon skipping were predicted by the EX SKIP tool contained in alamut visual [22]. Sanger sequencing of DNA extracted from PFA fixed renal tumor tissue and a peritoneal metastasis using primers adapted for short amplicons targeting the intron-exon border of exon 11, yielded c.1177-5_-3delCTC in an allegedly homozygous state. Since carcinogenesis in BHD syndrome is assumed to occur according to the Knudson's hypothesis sequencing findings most likely represented loss-of-heterozygosity with deletion of the second *FLCN* allele in tumor tissue (Fig. 2). To further investigate this finding we performed array CGH and MLPA analyses. While array CGH on tumor material proved inconclusive on a 180 k standard array, *FLCN* MLPA analyses were consistent with deletion of the second *FLCN* allele in both tumor tissues (data not shown).

Since the mutation had been reported before in association with the clinical diagnosis of BHD syndrome [4, 23, 24] and the family in the latter report only presented with asymptomatic pneumothorax respectively lung cysts and skin manifestation we decided to further evaluate the effect of this sequence alteration to confirm its pathogenic potential on a molecular level. To validate the mutation's impact on splicing of the FLCN transcript we generated minigene constructs containing either the *FLCN* wild-type (WT) or

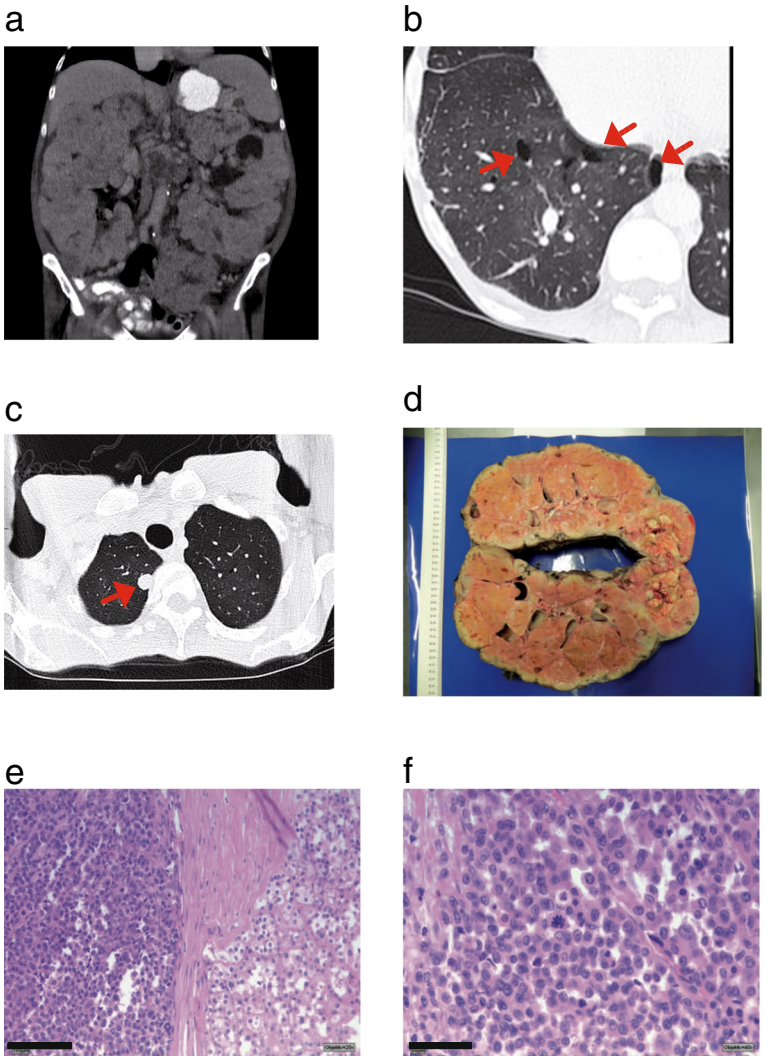

Fig. 1 CT imaging of the patient and macroscopic and histopathological analysis of the kidney tumor tissue **a** CT scan of the abdomen shows massive enlarged kidneys with bilateral tumorous lesions. **b** and **c** CT scan of the thorax reveals numerous pulmonary cysts (**b**, *red arrows*) and several pulmonary lesions suspicious for metastatic disease (**c**, *red arrow*). **d** Macroscopic picture of the left kidney shows that the whole organ is interspersed with nodular tumors. **e** Beside the nodular growing chromophobe carcinoma (right side) a second tumor component consisting of very small tumor cells can be detected (left side of the panel, bar = 100 μm). **f** these small tumors cells show nuclear pleomorphism with increased and atypical mitosis (bar = 50 μm)

the c.1177-5—3 del CTC (Mut) sequence. These minigene constructs encoding parts of human *FLCN* were transfected into mouse IMCD cells to prevent that the amplification of endogenous human *FLCN* interferes with our analyses. Minigene construct 1 (minigene-1) consisted of parts of exon 10, intron 10-11 with (Mut) or without (WT) the mutation and parts of exon 11. The analysis revealed that the 3 bp deletion indeed abrogated the acceptor splice site of exon 11 (Additional file 2: Figure S2). To further explore how the mutation affects the splicing of the *FLCN* mRNA we used a second minigene (minigene-2) that consisted of exon 10, intron 10 (with and without the 3 bp deletion), exon 11, intron 11, and exon12. Sequencing of the respective bands showed that the intronic 3 bp deletion CTC at position -7 to -5 leads to skipping of exon 11 and fusion of exon 10 (in frame) to exon 12 which generates a frameshift and premature stop codon (p.T393Sfs33*) (Fig. 3). Interestingly, in the WT minigene-2 construct, exon 11 was differentially spliced and partially skipped to a certain degree as well. This could also be observed with human cDNA of endogenous FLCN. Yet, the full-length wildtype splice variant was never observed when expressing the mutated version of minigene- 2 (Fig. 3).

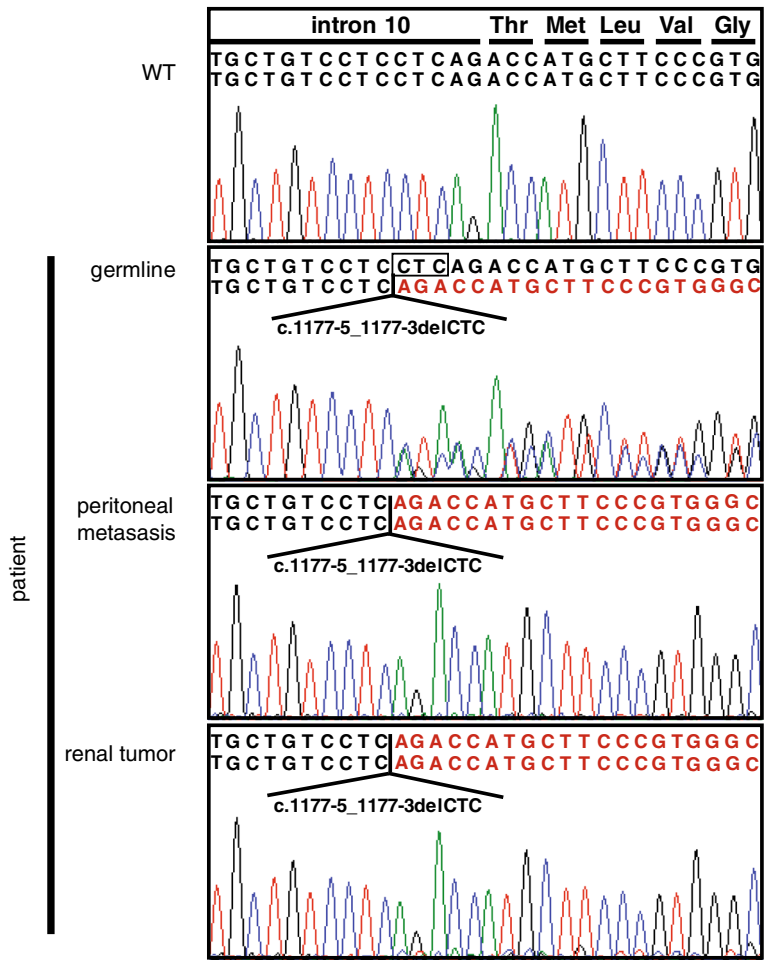

Fig. 2 Sanger sequencing of lymphocyte DNA of the patient reveal a heterozygous three nucleotide deletion in an intron *right upstream* of exon 11 (c.1177-5_1177-3). The same mutation was found in homozygous state when the renal tumor or the peritoneal metastasis was sequenced

To investigate whether the predicted FLCN neoprotein (p.T393Sfs33*, see Fig. 4a for an alignment of the protein sequences) is expressed at all we analyzed protein expression in HEK293T cells. Overexpression of a FLAG-tagged cDNA revealed that the mutant protein is expressed, however, at much lower levels than the WT protein (Fig. 4b and c). Since a commercially available anti-FLCN antibody (CellSignaling, #3697) detected the overexpressed mutant protein in Western Blots (Fig. 4c), we decided to use this antibody to analyze the endogenous expression in patient tumor tissue. SiRNA experiments and staining of the FLCN knockout cell line UOK257 as well as lentivirally transduced cells reexpressing FLCN revealed that the antibody specifically detected FLCN and could also be used for immune histochemistry (Additional file 3: Figure S3a and b). A distinct signal was obtained in the IHC analysis of the patient tumor indicating that expression of the mutant protein also occurs in vivo (Additional file 3: Figure S3c).

To confirm this finding we generated transgenic cell lines using the TALEN technology that express GFP-fused versions of either the WT or the mutant protein from the AAVS1-locus. This technology has the advantage of a single integration of the desired transgene into the genome, thereby resulting in expression levels that mimick the physiological situation more closely. Furthermore, since the transgenes were fused to GFP, imaging approaches are simplified. Whilst WT FLCN was easily detected by western blot the mutant protein again showed markedly lower protein levels (Fig. 5a and b). This effect could in part be reversed by treatment with MG-132 (Fig. 5a). Besides, treatment with chloroquine also increased the abundance of the mutant protein suggesting a combination of lysosomal and proteasomal degradation (Fig. 5b).

Additionally, fluorescence imaging revealed an altered subcellular localization profile of mutant FLCN in comparison to the WT protein. Whilst WT FLCN localizes to both cytoplasm and nucleus with a

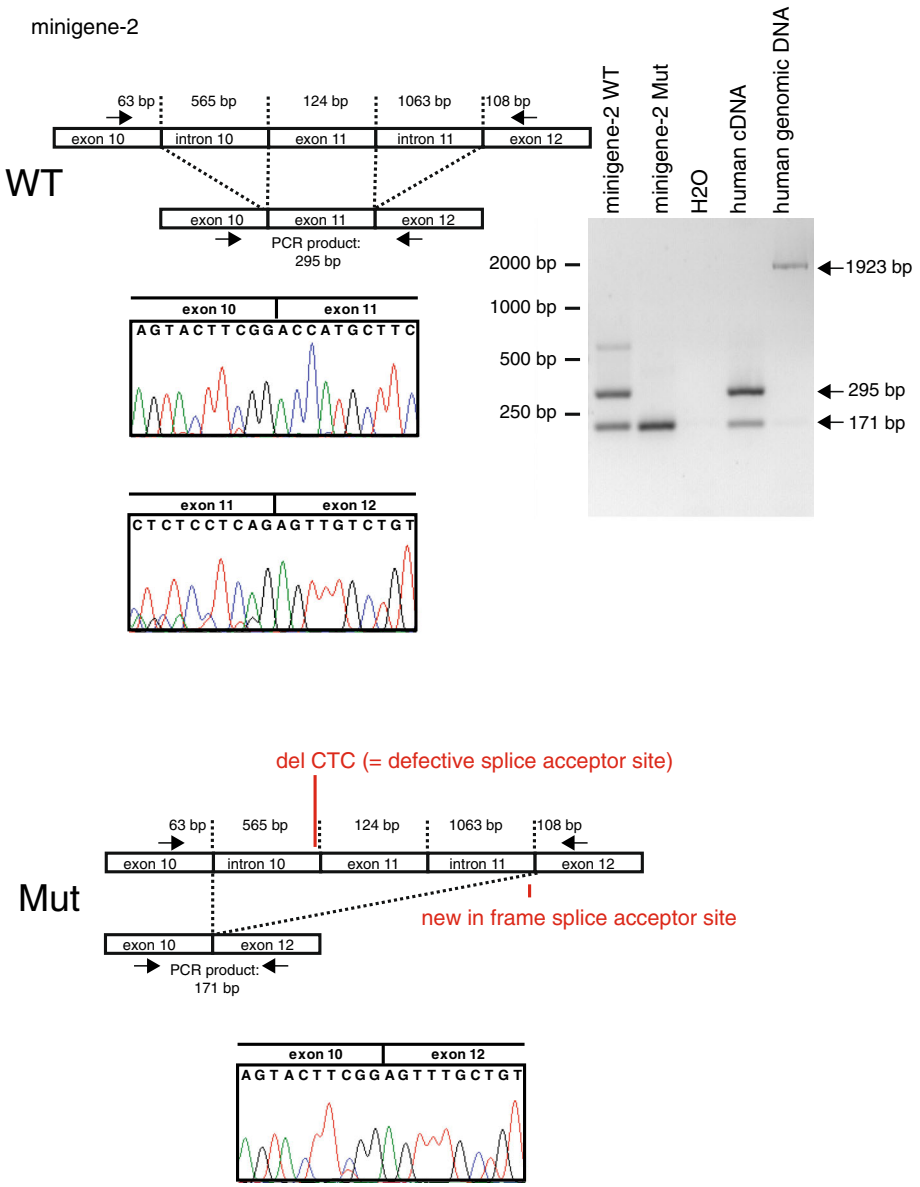

Fig. 3 To investigate the consequence of the patient mutation, minigene-2 was engineered (containing exon 10, intron 10, exon 11, intron 11 and exon 12 of human *FLCN*). After transfection into mIMCD cells (of mouse origin) RNA and afterwards cDNA was prepared and subjected to sequencing and PCR. As expected, the PCR using the WT minigene-2 results (the fp and rp are located in exon 10 and exon 12, respectively) in a band of 295 bp (expected size after splicing of intron 10 (=565 bp) and intron 11 (=1063 bp)). Analysis of the mutant minigene-2 reveals that - as expected - in addition exon 11 (=124 bp) is spliced out resulting in a smaller PCR product of 171 bp. Sequencing of the PCR products reveals, that the defective splice acceptor site in front of exon11 leads to skipping of exon11. Since the splice acceptor site of exon 12 is in frame, fusion of exon 10 and exon 12 can be detected. Interestingly, also with the WT minigene-2 as well as with human cDNA skipping of exon 11 can be observed. Human cDNA and human genomic DNA served as controls for the PCR products. Sanger sequencings confirmed the results, electropherograms of the crucial junctions are shown

very distinct nuclear signal the mutant protein is primarily restricted to the cytoplasm. Interestingly, treatment with MG-132 did not only stabilize the mutant protein but also led to a nuclear shift (Fig. 6) making its localization more similar to the WT situation.

Taking into account the genetic exam as well as the biochemical confirmation of pathogenicity and the autosomal dominant nature of BHD syndrome we invited the kindred of our patient to genetic counseling and testing which revealed other members of his family showing features of BHD syndrome to carry the mutation.

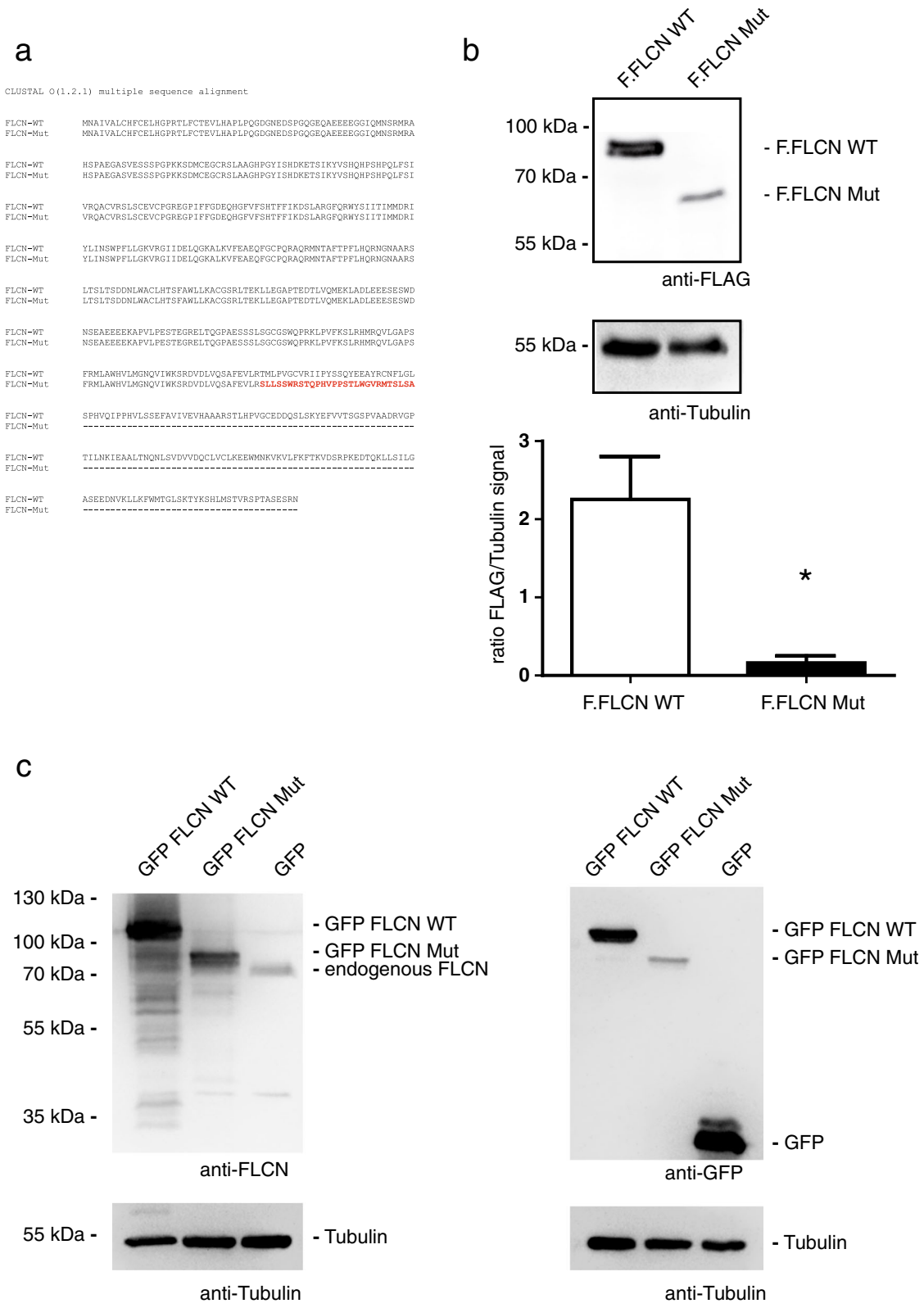

Fig. 4 (See legend on next page.)

(See figure on previous page.)
Fig. 4 a Alignment of the FLCN WT and FLCN mutant sequence on the protein level. The altered amino acid sequence caused by the mutation is shown in *red*. The alignment was peformed using ClustalOmega [36]. **b** Equal amounts of FLAG tagged FLCN WT or Mut plasmids were transfected into HEK293T cells and the expression level of both constructs was analysed using Western Blot. The mutant protein (Mut) is less expressed in comparison to the WT protein. Tubulin served as loading control. The results of three independent experiments were analysed by densitometry (n =3, error bars indicate SEM, * = $p < 0.05$, two tailed t-test).**c** The FLCN antibody (CellSignaling, #3697) detects the FLCN mutant (delta exon 11). HEK293T cells were transfected with GFP tagged FLCN wildtype (WT), the patient mutation (Mut) or GFP (control). Western blot analyses show that the FLCN antibody detects both the FLCN WT and Mut protein as well as endogenous FLCN (panels on the left side). Expression of all plasmids was verified using an anti-GFP antibody. Tubulin served as loading control

Discussion

Here we report a (familial) case of BHD with disseminated renal cell carcinoma and recurrent pneumothoraces in the index patient. Even though this can be regarded a classical picture of BHD syndrome there were a couple of unusual clinical as well as molecular aspects. First – even though present in about 90% of all BHD patients – physical examination results of the index patient did not describe a classical skin phenotype. Furthermore, in addition to the chromophobe RCC - the most common histology in BHD patients [25, 26] a poorly characterized small cell carcinoma was found upon histopathological analysis of the explanted kidney. BHD-syndrome associated renal cell carcinomas normally show a rather benign nature and rarely metastasize. Our patient suffered from both histologically confirmed peritoneal metastases and CT-morphological pulmonary lesions. The peritoneal metastases did not show the classical characteristics of the of the chromophobe RCC but rather resembled the less differentiated parts of this tumor showing a small-cell morphology. Since the chromophobe renal cell carcinoma showed different levels of dedifferentiation towards the areas of the small cell tumor component it is tempting to speculate that the small cell carcinoma arose from the chRCC by acquiring further genetic alterations. Furthermore, the metastasis appears to be linked to BHD syndrome since it showed loss-of-heterozygosity in the FLCN gene. It

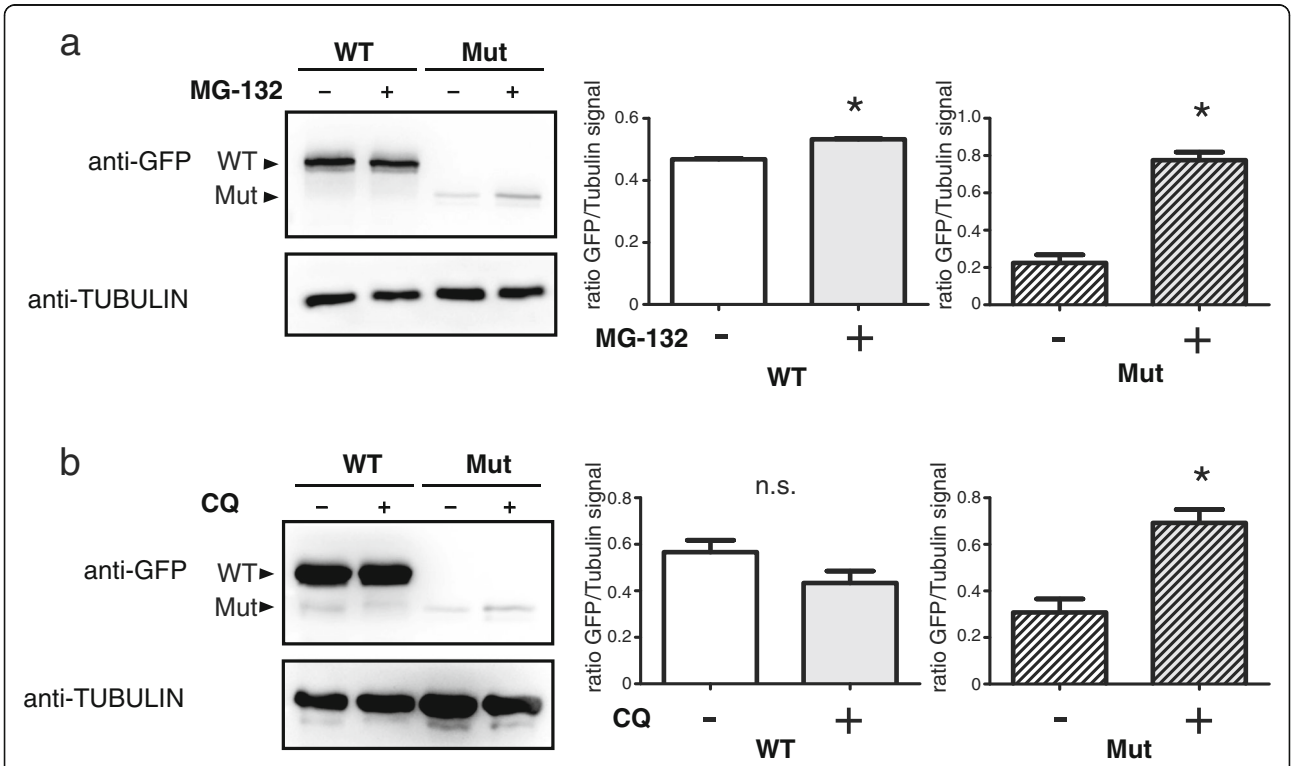

Fig. 5 To analyse the impact of the patient mutation on the protein level, HEK293T cells expressing FLCN WT or Mut fused to GFP using the TALEN technology were generated. **a** and **b** Western blot analyses reveals that the mutant protein is hardly expressed. This could in part be alleviated with MG-132 (**a**, treatment with 10 μM for 2 h) or chloroquine (**b**, treatment with 50 μM for 24 h), indicating an involvement of the proteasome and lysosome in the degradation process. Tubulin served as loading control (p =3, error bars indicate SEM, * = $p < 0.05$, n.s. = not significant, two tailed t-test)

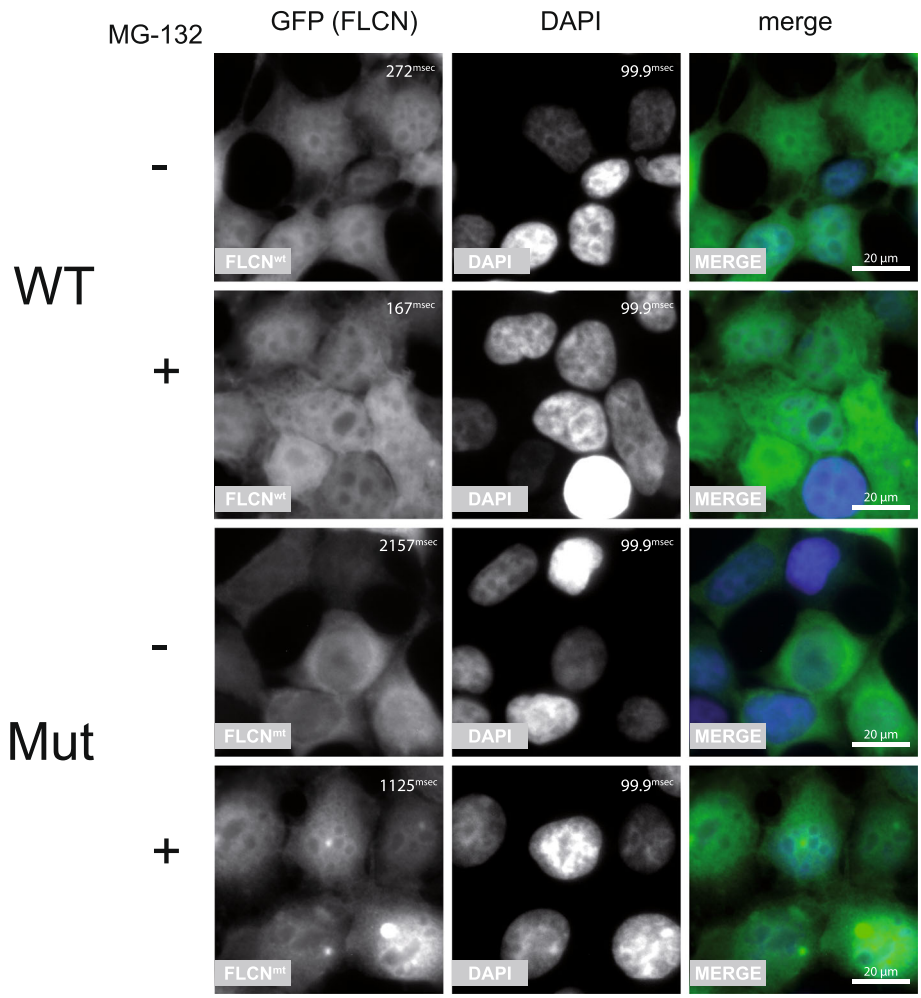

Fig. 6 HEK293T cells expressing FLCN WT or Mut fused to GFP using the TALEN technology were subjected to immunofluorescent imaging. WT FLCN localizes to both cytoplasm and nucleus, the mutant protein is primarily found in the cytoplasm. Interestingly treatment with MG-132 did not only stabilize the mutant protein which is reflected by a shorter exposure time during image acquisition but also led to a nuclear shift making its localization more similar to the WT protein (bar = 20 µm, exposure time of the GFP and DAPI channel are depicted in millisecond in the upper right corner of each panel)

will be interesting to see in future cases whether this entity is associated with BHD syndrome. Hybrid tumors are a common feature in BHD patients, although most of these contain chromophobe and oncocytomic cancer tissue. Clear cell carcinomas (ccRCC) have been described as well [25]. In our case no oncocytomas or ccRCCs could be detected in the explanted kidney. Interestingly, to our knowledge a small cell carcinoma component had not previously described in tumors of BHD patients.

The mutation detected in our patient had been found in patients fulfilling at least a subset of clinical features of BHD syndrome before [23, 24]. However, whether the intronic variant observed really leads to a change in the resulting protein had not been proven on a biochemical level. Our findings emphasize the fact that mutations in non-coding regions have to be taken into account when analyzing genetic diseases and have probably been underestimated so far. While this manuscript was under revision a Danish group characterized the same mutation that they found in two sisters with RCC using a minigene assay and essentially found the same results in regard to splicing of WT and mutant FLCN [27].

As described above the mutant protein was expressed at much lower levels than the WT version. Previously it had been shown that the FLCN complex localizes to lysosomes and granules containing ubiquitin. Furthermore, the FLCN interaction partner FNIP is regulated by SCFβ-TRCP [20, 28, 29]. Inhibition of both lysosomal and proteasomal degradation stabilized the mutant protein. Additionally, MG-132 also partly rescued its localization defect. This may be the consequence of

accumulation of ubiquitinated mutant FLCN, since ubiquitination has been shown to be a key regulator of subcellular localization of a number of different proteins [30–34]. Similar approaches have been hypothesized before as potential therapeutic strategies in genetic diseases [35]. Whether these approaches may have any therapeutic implication in the treatment of BHD – once stabilized and correctly localized - to fulfil the molecular function required to prevent tumorigenesis remains to be elucidated. Answering this question will require future studies in both cell culture and mouse models.

Conclusions

Whilst most mutations identified in BHD syndrome so far affect the coding region it is to be expected that a significant proportion of cases is caused by alterations in non-coding regions such as the intronic parts of splice sites. The pathogenicity of these mutations can often not be predicted as easily as alterations leading to classical nonsense or missense situations. Consequently, biochemical workup of the consequences of the sequence changes play an important role in the characterization of a novel mutation. Furthermore, even though chromophobe RCC is most common renal carcinoma entity found in BHD syndrome our case shows that other subtypes are possible and may be associated with a much more aggressive course of disease. Rescuing functional consequences of the mutations involved like altered localization through inhibition of ubiquitination may facilitate future therapeutic strategies to this familial disease.

Additional files

Additional file 1: Figure S1. Histopathological analysis of the kidney tumor tissue and histopathological work up of the peritoneal metastasis. **a** and **b** Histopathological analysis reveals chromophobe carcinoma in the kidney (a: bar = 1000 μm; b: bar = 50 μm). **c** Beside the nodular growing chromophobe carcinoma (right side) a second tumor component consisting of very small tumor cells can be detected (on the left side of the panel, bar = 1000 μm). **d** and **e** HE staining shows that the peritoneal metastasis consists of the small tumor cell component that was also found in the tumor tissue of the kidney (**d**: bar = 1000 μm; **e**: bar = 50 μm) **f** and **g** Ki-67 staining reveals a very high proliferation index in the small cell component of the peritoneal metastasis (**f**) as well as the small cell component of the kidney tumor (**g**) (**f**: bar = 50 μm, **g**: bar = 100 μm). (PDF 468 kb)

Additional file 2: Figure S2. Exon 10, intron 10 and exon 11 of *FLCN* were cloned into an expression vector. After transfection into mIMCD cells (of mouse origin) RNA and afterwards cDNA was prepared and subjected to sequencing and PCR. As expected in the wildtype (WT) situation, intron 10 (= 565 bp) is spliced out, resulting in a PCR product of 197 bp when using primers that are located in exon10 and exon11. The patient mutation leads to a not functional splice acceptor site in front of exon 11. As a consequence, intron 10 is not spliced out leading to larger PCR product of 762 bp. Human cDNA and human genomic DNA served as controls for the PCR products. Sanger sequencings confirmed the results, electropherograms of the crucial junctions are shown. (PDF 929 kb)

Additional file 3: Figure S3. a Western blots were loaded with whole cell lysates of cultured human cells (RPE-1) that had been transfected either with scrambled control siRNA or with two different siRNAs targeting FLCN. Staining with the anti-FLCN antibody shows one specific band at the expected molecular weight the intensity of which is strongly reduced by FLCN knockdown (left panel). Anti-Actin staining of the same membrane was used to control for equal loading (right panel). **b** To check whether the antibody was suitable for IHC as well we stained cell pellets of the established FLCN knockout cell line UOK257 lentivirally transduced to express emGFP (left image) showing little to no signal. UOK257cells that had been lentivirally transduced to express FLCN show a strong signal (magnification 40×). **c** IHC in human tissue shows that FLCN can still be detected in the chromophobe renal cell carcinoma of the BHD patient (middle panel). Normal human kidney tissue from a control (left side) was stained for comparison and shows a stronger signal. A control staining without the FLCN first antibody is shown on the right side of the panel (magnification 40×). (PDF 9710 kb)

Abbreviations

AAVS1: Adeno-associated virus integration site 1; AMPK: AMP-activated protein kinase; array CGH: Array comparative genomic hybridization; BHD: Birt-Hogg-Dubé; ccRCC: Clear-cell RCC; cDNA: Complementary DNA; CDX2: Caudal type homeobox transcription factor 2; chRCC: Chromophobe RCC; CK7: Cytokeratin 7; CKAE1/3: Pan cytokeratin; CT: Computed tomography; DNA: Deoxyribonucleic acid; FLCN: Folliculin; FNIP: Folliculin-interacting protein; fp: Forward primer; GFP: Green fluorescent protein; HCl: Hydrochloric acid; HEK: Human embryonic kidney cells; HGMD: Human gene mutation database; HIF: Hypoxia-inducible transcription factor; IHC: Immunohistochemistry; IMCD: Inner medullary collecting duct cells; Ki-67: Marker of proliferation Ki-67; LOVD: Leiden open variation database; MLPA: Multiplex ligation-dependent probe amplification; mTOR: Mechanistic target of rapamycin; Mut: Mutant; PAGE: Polyacrylamide gel electrophoresis; PCR: Polymerase chain reaction; PFA: Paraformaldehyde; PVDF: Polyvinylidene fluoride; RCC: Renal cell carcinoma; RNA: Ribonucleic acid; rp: Reverse primer; RPE-1: Retina pigmented epithelium cells; SDS: Sodium dodecyl sulfate; siRNA: Short interfering RNA; TALEN: Transcription activator-like effector nuclease; TGFb: Transforming growth factor beta; TTF-1: Thyroid transcription factor 1; VEGF: Vascular endothelial growth factor; VHL: Von-Hippel-Lindau; WT: Wildtype

Acknowledgments

We thank Kathrin Riehl and Martyna Brütting for excellent technical assistance and members of our laboratories for helpful discussion. UOK257 cells were a kind gift from Laura Schmidt and Michael Pollak (NIH).

Funding

This study was supported by the Nachwuchsgruppen. NRW program of the Ministery of Science Northrine-Westfalia (MIWF), Center for Molecular Medicine Cologne (GB-13), Deutsche Nierenstiftung and Deutsche Forschungsgemeinschaft (MU 3629/2-1) to Roman-Ulrich Müller. Malte P. Bartram was supported by an intramural grant of the University of Cologne (Gerok program).

Availability of data and materials

All data generated or analysed during this study are included in this published article and its Additional files.

Authors' contributions

MPB and TM contributed equally. MPB, TM and RUM conducted most of the experiments, analyzed data and wrote the manuscript. NR and BBB performed the analyses of patient DNA. FF and HGh performed experiments in cell culture. HG and ACA conducted the workup of patient tissue. MF and SH obtained the radiological images and derived the corresponding figures. TB and BS analyzed data and contributed to writing the manuscript. All authors read and approved the final manuscript.

Competing interests

The authors declare that they have no competing interests.

Consent for publication
Written informed consent regarding publication of the data was obtained from the patient.

Ethics approval and consent to participate
Since the data shown is not derived from a study but only involves a single patient and is published retrospectively the ethics committee was not involved. Written informed consent regarding scientific use of the data was obtained from the patient.

Publisher's Note

Author details
[1]Department II of Internal Medicine and Center for Molecular Medicine Cologne, University of Cologne, Kerpener Str. 62, 50937 Cologne, Germany. [2]Institute of Human Genetics, University of Cologne, Kerpener Str. 62, 50937 Cologne, Germany. [3]Department of Pathology, University of Cologne, Kerpener Str. 62, 50937 Cologne, Germany. [4]Department of Radiology, University of Cologne, Kerpener Str. 62, 50937 Cologne, Germany. [5]Dr. Hancken Clinic, Harsefelder Str. 8, 21680 Stade, Germany. [6]Cologne Excellence Cluster on Cellular Stress Responses in Aging-Associated Diseases (CECAD), University of Cologne, Cologne, Germany. [7]Systems Biology of Ageing Cologne (Sybacol), University of Cologne, Cologne, Germany.

Received: 26 October 2016 Accepted: 4 May 2017
Published online: 12 May 2017

References

1. Nickerson ML, Warren MB, Toro JR, Matrosova V, Glenn G, Turner ML, et al. Mutations in a novel gene lead to kidney tumors, lung wall defects, and benign tumors of the hair follicle in patients with the Birt-Hogg-Dubé syndrome. Cancer Cell. 2002;2:157–64.
2. Birt AR, Hogg GR, Dubé WJ. Hereditary multiple fibrofolliculomas with trichodiscomas and acrochordons. Arch Dermatol. 1977;113:1674–7.
3. Published BHD Families | Birt-Hogg-Dubé Syndrome [Internet]. [cited 2016 Aug 21]. Available from: https://www.bhdsyndrome.org/for-researchers/what-is-bhd/introduction/published-bhd-families/.
4. Lim DHK, Rehal PK, Nahorski MS, Macdonald F, Claessens T, Van Geel M, et al. A new locus-specific database (LSDB) for mutations in the folliculin (FLCN) gene. Hum Mutat. 2010;31:E1043–51.
5. Wei M-H, Blake PW, Shevchenko J, Toro JR. The folliculin mutation database: an online database of mutations associated with Birt-Hogg-Dubé syndrome. Hum Mutat. 2009;30:E880–90.
6. Houweling AC, Gijezen LM, Jonker MA, van Doorn MBA, Oldenburg RA, van Spaendonck-Zwarts KY, et al. Renal cancer and pneumothorax risk in Birt-Hogg-Dubé syndrome; an analysis of 115 FLCN mutation carriers from 35 BHD families. Br J Cancer. 2011;105:1912–9.
7. Toro JR, Wei M-H, Glenn GM, Weinreich M, Toure O, Vocke C, et al. BHD mutations, clinical and molecular genetic investigations of Birt-Hogg-Dubé syndrome: a new series of 50 families and a review of published reports. J Med Genet. 2008;45:321–31.
8. Vocke CD, Yang Y, Pavlovich CP, Schmidt LS, Nickerson ML, Torres-Cabala CA, et al. High frequency of somatic frameshift BHD gene mutations in Birt-Hogg-Dubé-associated renal tumors. J Natl Cancer Inst. 2005;97:931–5.
9. Knudson AG. Mutation and cancer: statistical study of retinoblastoma. Proc Natl Acad Sci U S A. 1971;68:820–3.
10. Schmidt LS, Linehan WM. Molecular genetics and clinical features of Birt-Hogg-Dubé syndrome. Nat Rev Urol. 2015;12:558–69.
11. Baba M, Hong S-B, Sharma N, Warren MB, Nickerson ML, Iwamatsu A, et al. Folliculin encoded by the BHD gene interacts with a binding protein, FNIP1, and AMPK, and is involved in AMPK and mTOR signaling. Proc Natl Acad Sci U S A. 2006;103:15552–7.
12. Baba M, Furihata M, Hong S-B, Tessarollo L, Haines DC, Southon E, et al. Kidney-targeted Birt-Hogg-Dube gene inactivation in a mouse model: Erk1/2 and Akt-mTOR activation, cell hyperproliferation, and polycystic kidneys. J Natl Cancer Inst. 2008;100:140–54.
13. Chen J, Futami K, Petillo D, Peng J, Wang P, Knol J, et al. Deficiency of FLCN in mouse kidney led to development of polycystic kidneys and renal neoplasia. PloS One. 2008;3:e3581.
14. Luijten MNH, Basten SG, Claessens T, Vernooij M, Scott CL, Janssen R, et al. Birt-Hogg-Dube syndrome is a novel ciliopathy. Hum Mol Genet. 2013;22:4383–97.
15. Preston RS, Philp A, Claessens T, Gijezen L, Dydensborg AB, Dunlop EA, et al. Absence of the Birt-Hogg-Dubé gene product is associated with increased hypoxia-inducible factor transcriptional activity and a loss of metabolic flexibility. Oncogene. 2011;30:1159–73.
16. Yan M, Gingras M-C, Dunlop EA, Nouët Y, Dupuy F, Jalali Z, et al. The tumor suppressor folliculin regulates AMPK-dependent metabolic transformation. J Clin Invest. 2014;124:2640–50.
17. Possik E, Jalali Z, Nouët Y, Yan M, Gingras M-C, Schmeisser K, et al. Folliculin regulates ampk-dependent autophagy and metabolic stress survival. PLoS Genet. 2014;10:e1004273.
18. Gharbi H, Fabretti F, Bharill P, Rinschen MM, Brinkkötter S, Frommolt P, et al. Loss of the Birt-Hogg-Dubé gene product folliculin induces longevity in a hypoxia-inducible factor-dependent manner. Aging Cell. 2013;12(4):593–603.
19. Tsun Z-Y, Bar-Peled L, Chantranupong L, Zoncu R, Wang T, Kim C, et al. The folliculin tumor suppressor is a GAP for the RagC/D GTPases that signal amino acid levels to mTORC1. Mol Cell. 2013;52:495–505.
20. Petit CS, Roczniak-Ferguson A, Ferguson SM. Recruitment of folliculin to lysosomes supports the amino acid-dependent activation of Rag GTPases. J Cell Biol. 2013;202:1107–22.
21. Folliculin mutations | Birt-Hogg-Dubé Syndrome [Internet]. [cited 2016 Aug 21]. Available from: https://www.bhdsyndrome.org/for-researchers/what-is-bhd/folliculin-gene/folliculin-mutations/.
22. Raponi M, Kralovicova J, Copson E, Divina P, Eccles D, Johnson P, et al. Prediction of single-nucleotide substitutions that result in exon skipping: identification of a splicing silencer in BRCA1 exon 6. Hum Mutat. 2011;32:436–44.
23. Kunogi M, Kurihara M, Ikegami TS, Kobayashi T, Shindo N, Kumasaka T, et al. Clinical and genetic spectrum of Birt-Hogg-Dube syndrome patients in whom pneumothorax and/or multiple lung cysts are the presenting feature. J Med Genet. 2010;47:281–7.
24. Kunogi Okura M, Yae T, Nagashima O, Hirai S, Kumasaka T, Iwase A. Pneumothorax developing for the first time in a 73-year-old woman diagnosed with Birt-Hogg-Dubé syndrome. Intern Med Tokyo Jpn. 2013;52:2453–5.
25. Pavlovich CP, Walther MM, Eyler RA, Hewitt SM, Zbar B, Linehan WM, et al. Renal tumors in the Birt-Hogg-Dubé syndrome. Am J Surg Pathol. 2002;26:1542–52.
26. Iribe Y, Kuroda N, Nagashima Y, Yao M, Tanaka R, Gotoda H, et al. Immunohistochemical characterization of renal tumors in patients with Birt-Hogg-Dubé syndrome. Pathol Int. 2015;65:126–32.
27. Rossing M, Albrechtsen A, Skytte A-B, Jensen UB, Ousager LB, Gerdes A-M, et al. Genetic screening of the FLCN gene identify six novel variants and a Danish founder mutation. J Hum Genet. 2017;62:151–7.
28. Nagashima K, Fukushima H, Shimizu K, Yamada A, Hidaka M, Hasumi H, et al. Nutrient-induced FNIP degradation by SCFβ-TRCP regulates FLCN complex localization and promotes renal cancer progression. Oncotarget. 2017;8:9947–60.
29. Xia Q, Wang G, Wang H, Hu Q, Ying Z. Folliculin, a tumor suppressor associated with Birt-Hogg-Dubé (BHD) syndrome, is a novel modifier of TDP-43 cytoplasmic translocation and aggregation. Hum Mol Genet. 2016;25:83–96.
30. Beck J, Maerki S, Posch M, Metzger T, Persaud A, Scheel H, et al. Ubiquitylation-dependent localization of PLK1 in mitosis. Nat Cell Biol. 2013;15:430–9.
31. Fryrear KA, Guo X, Kerscher O, Semmes OJ. The Sumo-targeted ubiquitin ligase RNF4 regulates the localization and function of the HTLV-1 oncoprotein Tax. Blood. 2012;119:1173–81.
32. Nakase M, Nakase Y, Chardwiriyapreecha S, Kakinuma Y, Matsumoto T, Takegawa K. Intracellular trafficking and ubiquitination of the Schizosaccharomyces pombe amino acid permease Aat1p. Microbiology. 2012;158:659–73.
33. McGehee AM, Strijbis K, Guillen E, Eng T, Kirak O, Ploegh HL. Ubiquitin-dependent control of class II MHC localization is dispensable for antigen presentation and antibody production. PLOS ONE. 2011;6:e18817.
34. Fang D, Kerppola TK. Ubiquitin-mediated fluorescence complementation reveals that Jun ubiquitinated by Itch/AIP4 is localized to lysosomes. Proc Natl Acad Sci U S A. 2004;101:14782–7.
35. Hofherr A, Wagner CJ, Watnick T, Köttgen M. Targeted rescue of a polycystic kidney disease mutation by lysosomal inhibition. Kidney Int. 2016;89:949–55.
36. Li W, Cowley A, Uludag M, Gur T, McWilliam H, Squizzato S, et al. The EMBL-EBI bioinformatics web and programmatic tools framework. Nucleic Acids Res. 2015;43:W580–4.